Moving contact line problem: Advances and perspectives

Yapu Zhao[a)]
State Key Laboratory of Nonlinear Mechanics (LNM), Institute of Mechanics,
Chinese Academy of Sciences, Beijing 100190, China

Abstract The solid–liquid interface, which is ubiquitous in nature and our daily life, plays fundamental roles in a variety of physical–chemical–biological–mechanical phenomena, for example in lubrication, crystal growth, and many biological reactions that govern the building of human body and the functioning of brain. A surge of interests in the moving contact line (MCL) problem, which is still going on today, can be traced back to 1970s primarily because of the existence of the "Huh–Scriven paradox". This paper, mainly from a solid mechanics perspective, describes very briefly the multidisciplinary nature of the MCL problem, then summarizes some major advances in this exciting research area, and some future directions are presented.

© *2014 The Chinese Society of Theoretical and Applied Mechanics.* [doi:10.1063/2.1403402]

I. INTRODUCTION

The static and dynamic properties of solid–liquid interfaces have been a topic of intense interest in many disciplines for a long time, such as materials science, chemistry, mechanics, biology, physics, etc. When a droplet is deposited on a substrate, the line where the interface between liquid and vapor intersects a solid substrate is named the contact line.[1] In Ref. 2, the Young's equation, published in 1805, is used to describe the static contact line's equilibrium configuration, and the three coefficients of interfacial tension is related to the contact angle formed by the liquid–vapor interface intersecting the solid surface. The problem of moving contact line (MCL) has found wide applications in industry such as micro- and nano-fluidics, bio-engineering, petroleum, chemical engineering, and so on. Nevertheless, for many years, the MCL problem has remained an issue of debate and controversy even at the macroscopic level. The main difficulty stems from two paradoxes: (1) the fact that classical hydrodynamic equations, which is coupled with the conventional no-slip boundary condition, predict a singularity for the stress and a logarithmic singularity for the energy dissipation rate at the liquid/vapor/solid triple contact point, as stated in the "Huh–Scriven paradox" (as shown in Fig. 1(a)) that "not even Herakles could sink a solid";[3] (2) the fact that the logarithmic singularity for the thermal energy dissipation rate at the liquid/vapor/solid triple contact point for the evaporation of a droplet, as stated in the "droplet evaporation paradox" (as shown in Fig. 1(b)) that "not even Helios could evaporate a water droplet".[1]

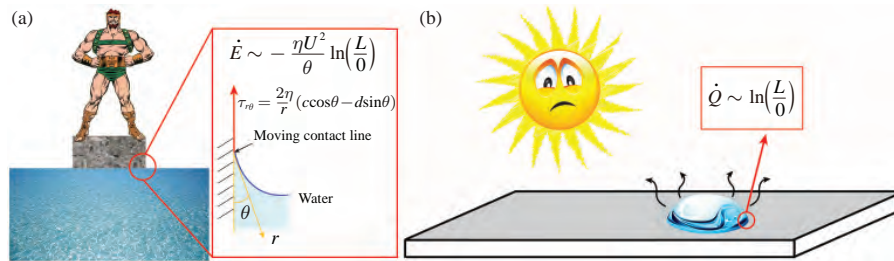[a)]Corresponding author. Email: yzhao@imech.ac.cn.

Fig. 1.   The two paradoxes in MCL problem: (a) Huh–Scriven paradox and (b) droplet evaporation paradox.

As shown in Fig. 2, the study of the solid–liquid interfaces and the MCL problem is inherently multidisciplinary. The phrases and terms in red color in Fig. 2 have direct relation with this review. For example, one can use the electrowetting to manipulate a water droplet, one can also wrap a water droplet by a flexible elastic sheet which is termed "elasto-capillarity (EC)". In recent years, we have systematically investigated the multi-scale and multi-field MCL problem by using multi-scale experiments and molecular dynamics (MD) simulations. Based on this study, we put forward and realized the electro-elasto-capillarity (EEC), further extended the molecular kinetic theory (MKT) model to the electrowetting and cell adhesion problems, found some new flow patterns at the interior corners, and formulated a new slip boundary condition for the MCL problem. This review will mainly summarize the advances of the study of the author's group on MCL problems, and some perspectives will also be presented concerning the MCL problem.
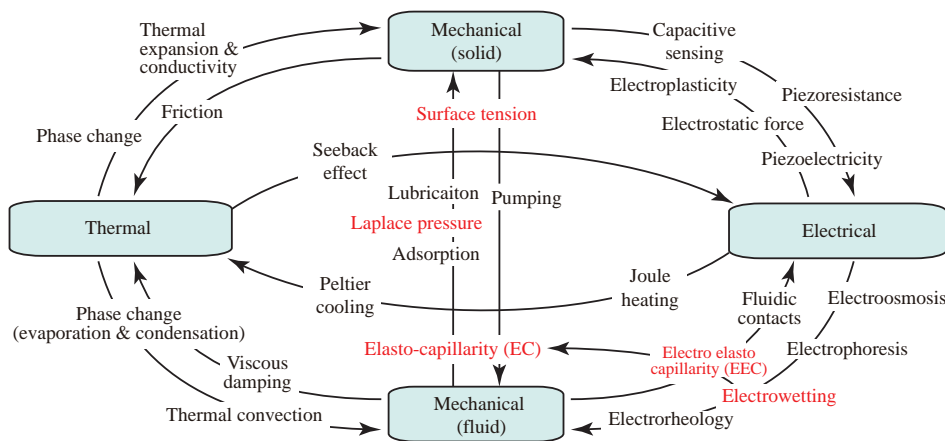

Fig. 2.   Multidisciplinary nature of the solid–liquid interface investigation.

II.   PRECURSOR FILM UNDER ELECTRIC FIELD AND EEC BY MD SIMULATIONS

A precursor film (PF), i.e., a very thin molecular layer, propagating ahead of the nominal MCL, plays an important role for not only the liquid, polymer or metal droplet, but also biologi-

cal cells in the spreading process.[4–6] The existence of PF was first predicted in Hardy's pioneering work.[7] Then, numerous theoretical and experimental studies on the spreading droplet have validated Hardy's results.[1] We carried out a multi-scale experimental investigation on the droplet spreading, which is shown in Fig. 3. The liquid droplet is a solution of hyperbranched polymer nanoparticles dissolved in chloroform with a volume of 0.33 μl. The solid substrate is the freshly cleaved muscovite mica (V-1, Electron Microscopy Sciences, USA) with a surface roughness on the scale of several angstroms. Since the chloroform is conveniently volatile, experiments were performed in water environment. The apparent contact angle was measured using an OCA20 system (precision $\pm 0.1°$, from Dataphysics, Germany), $\theta_{ap} = 35.1°$ (Fig. 3(b)). For the actual contact angle, it was estimated based on the optical interference principle, $\theta_{ac} \approx \lambda/(2nb)$, in which λ is the incident wavelength, n is the refractive index, and b is the fringe spacing. Analyses on the results presented in Fig. 3(c) show that $\theta_{ac} \approx 2.5°$. To study the spreading of PF, atomic force microscopy (AFM) (Agilent-5500) was used to scan the molecular region, as shown in Figs. 3(d)–3(f). Regular surface roughness was found in this region, which is consistent with the diameter of the dissolved nanoparticles (2–3 nm). The comparable experimental observation verifies the muli-scale spreading of liquid droplets described in Fig. 3(a).
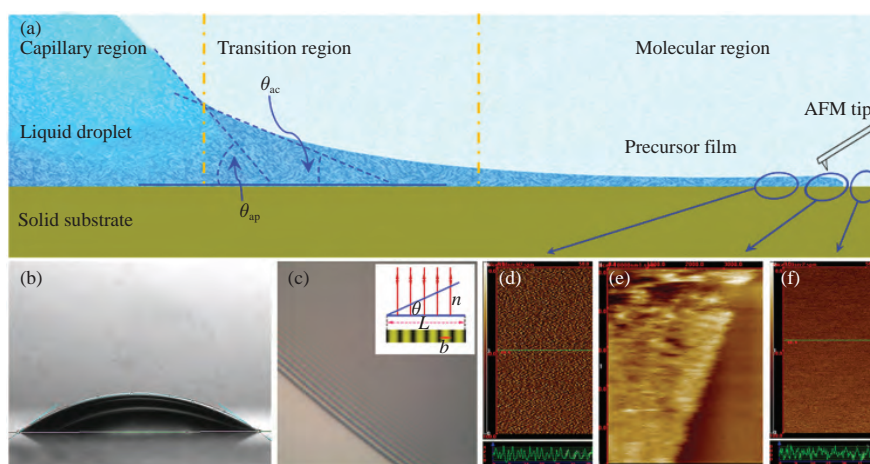

Fig. 3.   Multi-scale experimental investigation on the droplet spreading: (a) schematic of the multi-scale spreading, (b) sessile liquid droplet on the solid substrate, (c) interference fringes in the transition region, (d) dissolved nanoparticles visualize the PF on the atomically smooth surface, (e) observed step indicating the tongue of the PF, and (f) AFM images of the mica surface.

The unphysical stress singularity as stated clearly in the "Huh–Scriven paradox" is due to the negligence of microstructures at the solid–liquid interface.[8] PF, a microstructure ahead of the nominal MCL, is just an answer to the Huh–Scriven paradox. Meanwhile, we find that PF is also the first answer to the stress singularity in electrowetting.[9]

The PF is generated by the disjoining pressure $\Pi(h) = A/(6\pi h^3)$, the thickness of PF was estimated by Hervet and de Gennes[10] to be $h_{PF} = a\sqrt{3\gamma_{lv}/2S}$, where $a = \sqrt{A/(6\pi\gamma_{lv})} \sim 10^{-10}$ m, γ_{lv} is the liquid–vapor interfacial tension, and A and S are the Hamaker constant and the spreading coefficient, respectively. The length of PF $L = 0.69 h_{PF}/Ca^{2/3}$ is related to the capillary number
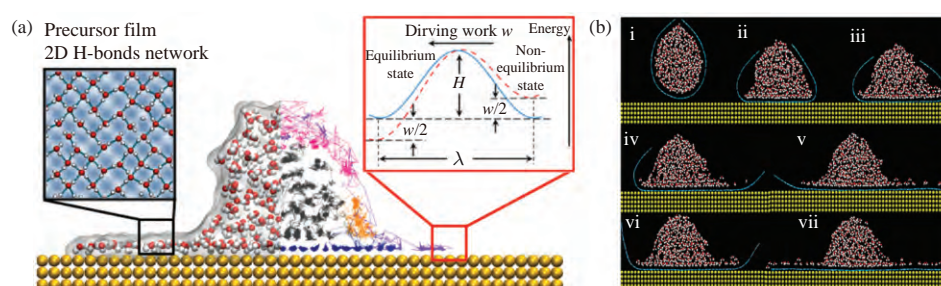
Fig. 4.   (a) Path lines of water molecules when a water droplet spreads on a smooth hydrophilic solid. (b) EEC.

$Ca = \eta U / \gamma_{lv}$, where η and U are the viscosity and velocity, respectively. PF is confined between the solid and the liquid, and is a kind of confined liquid, which exhibits the properties of layering and solid-like.[1]

When a droplet was deposited on a smooth hydrophilic solid, PF spread fast ahead of the rest of the liquid and formed a thin liquid film on the solid, then the bulk droplet spread on the base of the PF (Fig. 4(a)). The droplet finally reached an equilibrium state described by the Young's equation.[2] To imitate the usual setup of electrowetting with typical electric field $E \sim 10^7$ V/m, the solid atoms were applied with increasing charges. The wettability of the solid surface increased with the increase of E. We tracked each of the water molecules when a water droplet spread on the smooth solid, and some of the path lines were taken to obtained Fig. 4(a). The new features of PF under electric field[9] are shown in Fig. 4(a). (1) The bulk water molecules (grey) were shown for comparison, which randomly diffused under thermal energy. (2) The surface molecules (pink) had the highest mobility. Because the liquid–vapor interface energy was weaker than the liquid–liquid interaction, the surface molecules moved quickly on the surface. (3) The water molecules in PF (blue) had the lowest mobility. PF molecules hopped around adsorption sites with a amplitude less than 0.3 nm. (4) Some water molecules (purple) moved fast at the surface. But once diffusing into the MCL region, they were pinned by the solid and became part of the PF. Since the surface molecules diffuse continuously and fast to PF, the PF propagates fast and dissipates with low energy. The path lines in electrowetting validated this conclusion again. The unique 2D hydrogen bonds (H-bonds) network in PF results in its unique transport behavior: it is harder for the water molecules to diffuse in PF, while it is easier to diffuse above PF. The diffusion coefficient D of the water molecules was calculated by Einstein relation. When the droplet spread, it has $D = 1.132 \times 10^{-5}$ cm^2/s in PF, which was 50.4% of $D = 2.246 \times 10^{-5}$ cm^2/s of the bulk water,[11] while D of the surface region was 7.354×10^{-5} cm^2/s. When the external electric field was imposed, D decreased to the orders of 10^{-6} cm^2/s (about 6% of D of the bulk water). These results indicate the solid-like feature of the PF.

We used for the first time the electric field to open the wrapped droplet, which is termed EEC,[9] as shown in Fig. 4(b) by using the unique transport properties of the PF (i.e., solid-like and fast spreading). First, we used graphene, whose radius is larger than the elasto-capillary length to wrap the droplet.[12] Then, an external electric field $E = 0.544$ V/nm along the $-y$ direction was

applied to unwrap the droplet, as shown in Fig. 4(b). Because of the faster propagation of PF compared with the bulk liquid, as well as the solid-like property of PF, PF pushed the graphene to unwrap with a force of the order of 1 nN/nm from our MD simulations. So by employing the unique transport properties of PF, EEC can be realized at micro/nano scale.

The dynamic wetting of topologically structured surfaces is of significant interest in both theoretical studies and applications.[13,14] However, the underlying mechanisms are far from being well understood. The dynamic wetting of a droplet on a pillar-arrayed surface is essentially a multiscale process as shown in Fig. 5(a).[15] At macroscopic level, when a droplet was deposited on pillars, the fringe penetrated into the space among the pillars and its spreading depended on the arrangement of pillars, while the bulk water spreads on the base of the fringe and its spreading is isotropic. The fringe superwetted the pillars and spread faster than the bulk. At mesoscopic level, driven by the hydrodynamic pressure, the fringe advanced in the forest of the pillars and formed a zigzag MCL. On one hand, the excess solid–liquid interface provided excess driving force to the liquid; on the other hand, the pillars bring excess resistance to the fringe. At microscopic level, a thin PF propagated ahead of the nominal MCL. Driven by the disjoining pressure, (1) PF rapidly evolved on the pillar surfaces; (2) two PFs encountered at the interior corner formed by the pillar and substrate and jetted a single-file precursor chain (PC).[16] The potential surface at the interior corner was lower and smoother than that on the smooth surface. Hence, the PC propagating ahead of the PF at the interior corner was more stable, bore less friction and propagated faster than the PF with respect to the interior angle. A 1D H-bonds network in PC was formed to transfer driving energy to push the solid-like PC to slip in the corner, and behaved just like a 1D H-bonds network in carbon nanotube, which makes a fast transport and has large slip length at the solid–liquid interface.[17]
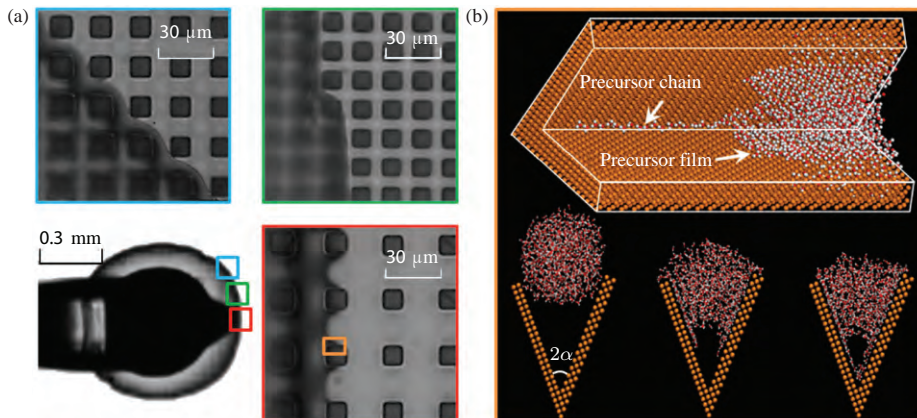

Fig. 5. Multiscale dynamic wetting of a droplet on a topologically structured surface.

We adopted the MKT, which was proposed by Glasstone et al.[18] to explain the physical mechanism behind these phenomenon. For the water molecules hop between solid sites separated by a distance λ with frequency κ_0, the advancing velocity $U = 2\kappa_0 \sinh(w\lambda^2/(2k_BT))$, where w is the work per unit area done by the driving force. According to Blake and de Coninck,[19]

$\kappa_0 = k_B T \exp(-\lambda^2 W_a/(k_B T))/(\eta v_m)$, where k_B is the Boltzmann constant, T is the absolute temperature, W_a and v_m are the work of adhesion between the solid and the liquid, and the molecular flow volume, respectively. In our cases, the driving work is less than the thermal energy, so we obtain the spreading velocity as

$$U = 2\frac{k_B T \lambda}{\eta v_m} \exp\left(-\frac{\lambda^2 W_a}{k_B T}\right) \sinh\left(\frac{w\lambda^2}{2k_B T}\right) \sim \frac{w\lambda^3}{\eta v_m} \exp\left(-\frac{\lambda^2 W_a}{k_B T}\right). \tag{1}$$

(1) **Wetting on a solid surface**[15]   The driving work arises from the interface energy $w = (\gamma_{sv} - \gamma_{sl})ro - \gamma_{lv}\cos\theta$, where γ_{sv} and γ_{sl} are the solid–vapor and solid–liquid interfacial energies, respectively, ro is the roughness of the solid surfaces, and θ is the instant contact angle. Taking account of the Young's equation ($\gamma_{sv} - \gamma_{sl} = \gamma_{lv}\cos\theta_0$, θ_0 is the static contact angle) and the lubrication approximation ($\theta \sim H/R \sim 0$),[20] spreading velocity the approximation as $U \sim \gamma_{lv}\cos\theta/\eta \sim \gamma_{lv}\theta^2/\eta$. For the sake of mass conservation, θ is close to $(8R_0^3/3R^3) - 2(1 - \phi_s)h/R$, where R_0 and R are initial and instant radii of the droplet, respectively. For rough surface, h and ϕ_s are the pillar height and the density of roughness, respectively. We can obtain scaling laws for the smooth and the rough surfaces, respectively. For spreading on smooth solid surface, it has $R/R_0 \sim (t/\tau_c)^{1/7}$. The characteristic time $\tau_c = \eta R_0/\gamma_{lv}$ is controlled by R_0 and capillary velocity $U_{ca} = \gamma_{lv}/\eta$. For spreading on rough surface, it has $R/R_0 \sim (t/\tau_c')^{1/3}$, where the characteristic time $\tau_c' = \eta R_0^3/(\gamma_{lv}\overline{h}^2)$ is controlled not only by properties of the bulk water, but also by the topological parameters of the rough surface: ϕ_s and $\overline{h}$ (the effective height of the pillars).

(2) **Wetting in an interior corner with opening angle 2α shown in Fig. 5(b)**[16]   Consider a special case along the angular bisector, $\theta = 0$, the work done by the disjoining pressure is

$$w(\alpha) = \frac{A_{Au\text{-}Water}}{48\pi} \sin^2\alpha \left(3\cot\left(\frac{\alpha}{2}\right) + \cot^3\left(\frac{\alpha}{2}\right)\right)\left(r_1^{-2} - r_2^{-2}\right),$$

where $A_{Au\text{-}Water}$ is the Hamaker constant between gold substrate and water. Because of the existence of PC, r_1 could not reach 0, but equals $\sigma_{Au\text{-}Water}$ ($\ll r_2$), so w is not sensitive to r_2. We adopted $r_2 = 5$ nm (the width of interior corner). W_a could be directly obtained from the MD simulations. With the increase of the interior angle, the driving work decreases and W_a increases. So, the spreading velocity decreases with the increase of the opening angle of the interior corner.

(3) **Electrowetting on a solid surface**[9]   In the case of electrowetting, an additional average electric energy w_E describing the interaction between electric field **E** and electric dipole moment **μ_i** is

$$w_E \sim \sum_i (-|\boldsymbol{E}||\boldsymbol{\mu}_i|L(|\boldsymbol{E}||\boldsymbol{\mu}_i|/(k_B T))),$$

where $L(x)$ is the Langevin function.[21] w_E is complicated for an electrowetting system and makes Eq. (1) have no analytical solution. So we used a power law $R \sim t^{n(E)}$ to fit the relationship between R and t. When E is larger than a critical electric field E_c, $n(E)$ begins to increase with E. And when E is larger than a saturated field E_s, $n(E)$ also saturates. These findings are validated

by relevant experimental observations.[22] We find that PF is the first answer to the Maxwell stress singularity in electrowetting.[9]

III. EXPERIMENTAL REALIZATION OF EEC

As shown in Fig. 4(b), we realized the EEC dynamics by MD simulations. As a matter of fact, flexible substrate devices become popular today, because of its advantages in wearable and portable devices. However, due to the flexibility of the materials, the vertical component of the capillary force may cause vertical deformation of the substrate,[1] which is not usually seen upon silicon or glass based devices. EC and EEC are such kinds of phenomena.[1] In 2004, Bico et al.[23] published a paper in *Nature*, reporting the mechanism of a common phenomenon in our daily life: coalescence of wet hair (Fig. 6(a)). Due to the surface tension of droplet, hairs are bent and get into bundles, and this process is named as EC. EC spontaneously occurs when the size of droplet has exceeded the elastocapillary length. Some groups also reported that EC could lead to a remarkable deformation in various types of flexible substrates (Fig. 6(c)), such as PDMS films, micro scale devices or graphene films (in MD simulation).[24–28]
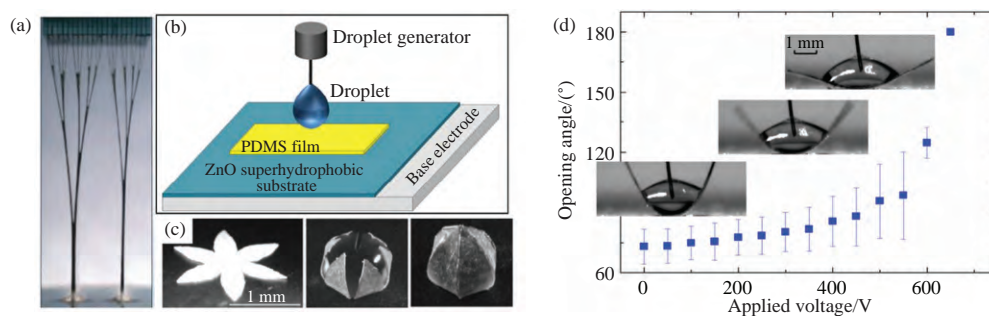

Fig. 6.   From EC to EEC. (a) Hair get bundled when it is wet. (b) Schematics of EEC experimental setup. (c) A droplet encapsulated by PDMS film. (d) With the increase of voltage, the thin film tends to release the droplet.

Based on EC, Zhao's group realized the opening of the wrapped droplet by applying an electric field in experiments,[29] and this new phenomenon was termed EEC,[9] which is a controllably encapsulation and release method of tiny droplets. EEC has introduced electric field into the droplet-thin film system, so that the deformation of substrate and droplet can be properly controlled. In experiments, direct current (DC) voltage and alternating current (AC) voltage have been applied upon a wrapped droplet. With the increase of voltage, the encapsulated droplet was released, and the system returned to the initial states (Fig. 6(d)).

Conductive salty liquid was used in the experiment and the droplet was located on the surface of a flexible thin (70 μm thick) PDMS film (Fig. 6(b)). The film was placed on a ZnO superhydrophobic surface, in order to minimize the adhesion force between substrate and thin film. When electric field is applied with, the PDMS film tended to unwrap the drop, due to the joint effect of Coulomb force, elastic force, and surface tension. When a critical value (∼650 V in the experiment) of the voltage is reached, the film was pulled-in to the substrate and the droplet is released

completely.

In the case of AC actuation, the droplet began to vibrate, just as it is tap-dancing (Fig. 7(a)), so AC actuated EEC is also called as "Tap dance of water droplet".[29] The frequency doubling effect was observed in this process. By deriving the Lagrangian equation of the system, the theoretical model is set up as

$$2I\frac{\mathrm{d}^2\Theta}{\mathrm{d}t^2} = \underbrace{-\frac{4Bw\Theta}{l_1}}_{\text{Bending energy}} \underbrace{-\frac{\gamma_{\text{lv}}wl_1\Delta}{\sin\Delta}\frac{\Theta\cos\Theta-\sin\Theta}{\Theta^2}}_{\text{Surface energy}} \underbrace{-\frac{\pi\varepsilon w\sqrt{l_1/h'}V_0^2\sin^2\omega t}{4\Theta^{3/2}}}_{\text{Electric energy}} \underbrace{-C\frac{\mathrm{d}\Theta}{\mathrm{d}t}}_{\text{Dissipation}}, \quad (2)$$

$$\underbrace{\phantom{2I\frac{\mathrm{d}^2\Theta}{\mathrm{d}t^2}}}_{\text{Kinetic energy}}$$

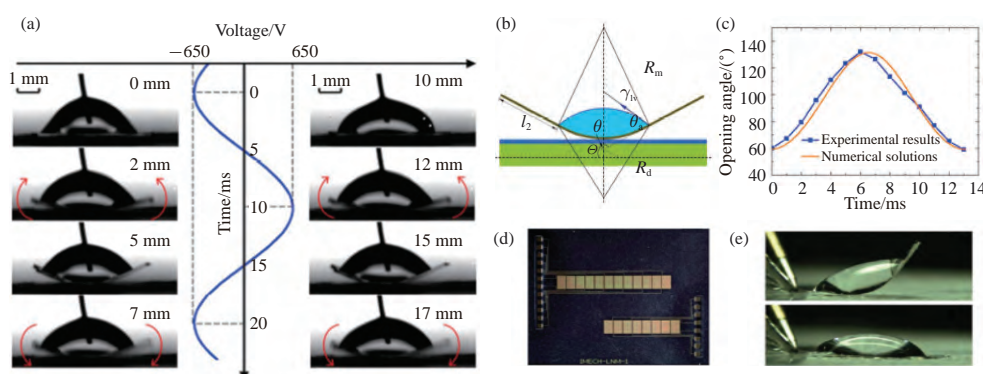where the parameters in Eq. (2) can be found in Ref. 29 (Figs. 7(b) and 7(c)).

Fig. 7.   EEC under AC voltage and its possible application in MEMS device actuation. (a) Droplet and thin film dance to the applied voltage. (b) Schematic of experiment and the parameter used in the model. (c) Theoretical model shows good accordance with experiments. (d) Micro devices fabricated upon Parylene thin film. (e) With increase of voltage, cantilever deflection is altered.

A micro-EEC device was also designed and fabricated in the author's group. Golden conductive electrodes were buried in a Parylene cantilever (Fig. 7(d)). By adding a water droplet to the surface of the cantilever, the device was bent upwards. Then, electric field was applied to the cantilever, and the bent cantilever became flat (Fig. 7(e)). By utilizing this method, the deflection can be controlled by electro static force, surface tension and elastic force.

EEC could be a potential off-plane actuation method of MEMS devices, since the surface tension tends to be a dominant interaction when the scale goes down. It is also a practical solution to protect tiny amount of liquid sample from being evaporated and polluted, in ultra-sensitive bio-medical sensors.

IV.   BOUNDARY SLIP

Although the Navier–Stokes equations form the basis of our understanding of the simple liquid flow, the boundary condition is another core concept in fluid mechanics. With a rich history rooted in interface science and recent advances in micro- and nano-fluidics technology, boundary slip

has recently been investigated for a rapidly increasing number of applications.[30] Boundary slip is fundamentally characterized by the fact that there is a relative motion between the fluid and the solid. Navier himself proposed a linear expression for the slip velocity, $V_s = l_s \dot{\gamma}$, in which l_s denotes the slip length with a constant value, and $\dot{\gamma}$ is the shear rate. Thus, slip velocity and slip length are used to quantify the boundary slip, as illustrated in Fig. 8.
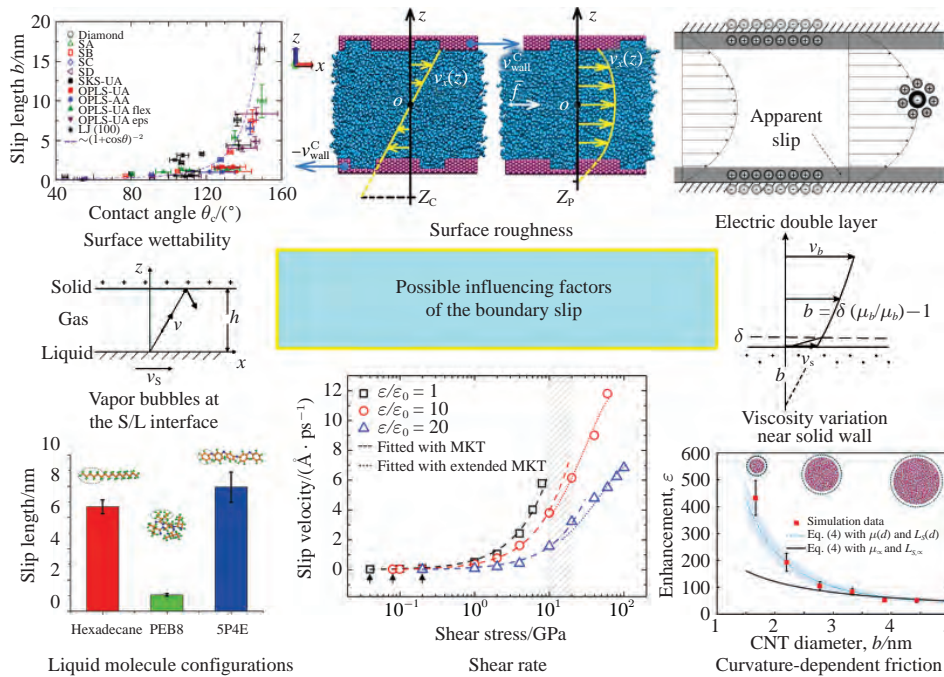

Fig. 8.   Illustration of the boundary slip, the MKT slip model as well as the possible influencing factors, including the surface roughness,[31] the nanoscale vapor bubbles generated at the liquid–solid interface,[32] the electric double layer,[33] the channel curvature dependent friction,[34] the shear rate,[35,36] the shape and the arrangement of the liquid molecules,[37,38] the wettability of the solid surface,[39] and the variation of viscosity near the solid walls.[40]

Boundary slip, according to the definition above, becomes extensively significant when referring to the micro- and nano-scale flow, which is of fundamental physical interest and is practically applicable widely in many areas, from designing nanofluidic devices to interpreting the biological ionic channels.[30] Since boundary slip is an interfacial behavior that relates the liquid flow and the solid wall, its influencing factors can be divided into three categories, as summarized in Fig. 8. Concerning the solid wall, researchers have discussed the effect of the surface roughness,[31] the nano-scale vapor bubbles generated at the liquid–solid interface,[32] the electric double layer,[33] and the channel curvature dependent friction.[34] For the part of liquid, we focus on the exerted shear rate,[35,36] and the liquid properties such as the shape and the arrangement of liquid molecules.[37,38] Besides, the liquid–solid coupling effect also contributes to the boundary slip, for example, the wettability of the solid surface,[39] and the variation of viscosity near the solid walls.[40] A new slip model has been recently proposed based on the Frenkel–Eyring MKT.[36] This

extended MKT slip model introduces a concept of critical shear stress, which determines the onset of the slip, and also considers the energy dissipation near the liquid–solid interface at high shear stresses. The new MKT slip model characterizes the slip behavior over a wide range of shear stress, and it is divided into three regimes. (1) No-slip regime. The boundary slip would not occur unless the critical shear stress is reached. It is found that the critical shear stress increases exponentially with the liquid–solid interactions, which can be confirmed in the MKT theoretical prediction and MD simulations. (2) Navier slip regime. When the shear stress is larger than the critical shear stress and not very high yet, the boundary slip occurs with a constant slip length. Within this regime, the MKT slip model can be reduced to the Navier's slip model. (3) Shear-dependent slip regime. The slip length increases with the shear rate. At even higher shear stress level, two different kinds of nonlinear responses are displayed by the shear-dependent boundary slip according to the wetting conditions of the solid surface. A dissipation factor is introduced into the MKT model to take account of the energy dissipation arising from the relative sliding between the individual liquid layers near the interface. A dimensionless modified Galilei number was suggested for comparing the relative importance of the intrinsic viscous force and the exerted driving force of the liquid, which is dominating in the nanoscale force-driven flow. This MKT slip model provides a definite expression of the amount of slip and can be used to characterize the slip behavior over a large range of shear stress, which can be compared with other existing slip models.[35,41]

Despite the aforementioned notable progress, the boundary slip still has some unclear and controversial aspects, that are yet to be adequately resolved. Firstly, a comprehensive MKT-based slip model which could include all the influencing factors should be explored in the future. Secondly, the thermostats in MD simulations of highly confined channel flow may significantly affect the fidelity of transport phenomena.[42] Therefore, the effects of the thermostat implementations should be fully understood.

V. PROPERTIES OF GRAPHENE–WATER INTERFACE UNDER ELECTRIC FIELDS

The property of graphene–water interface is most important for realizing the applications of graphene because it not only defines the interaction between graphene and its environment but also directly impacts the properties of graphene. For example, the wettability of graphene was reported to affect the energy storage capacity of a graphene super-capacitor,[43] and the adsorbed water film on graphene can open the bandgap of graphene.[44] Recently, Li et al.[45] have found that the freshly graphene surface is hydrophilic, which subverts the generally accepted knowledge that supported graphene is hydrophobic, and they suggested that previously reported data may have been affected by unintentional hydrocarbon contamination from ambient air. This further illustrates the importance of water adsorption on graphene surface. While much progress has been made, the application of graphene in electronic devices deserves further investigation of graphene–water interface under an electric field.

Zhao's group[46] explored the properties of graphene–water interface under the electric field considering both the deformation of graphene and the structure of the adsorbed water. A water

droplet was firstly placed on the graphene with zero charge. Under the vertical component of surface tension, the droplet was spontaneously wrapped by the graphene. Then, an electric field was applied to release the droplet as shown in Fig. 9(a). Under the electric field, some water molecules were attracted to the graphene and others to the substrate to form two PFs. The upper PF propagated to unwrap the folding graphene and the lower PF propagated to delaminate the graphene from the substrate (Fig. 9(b)). During this process, two PFs compete in the form of capillary wave. The physics of the capillary wave was explored by MKT (Fig. 9(c)).
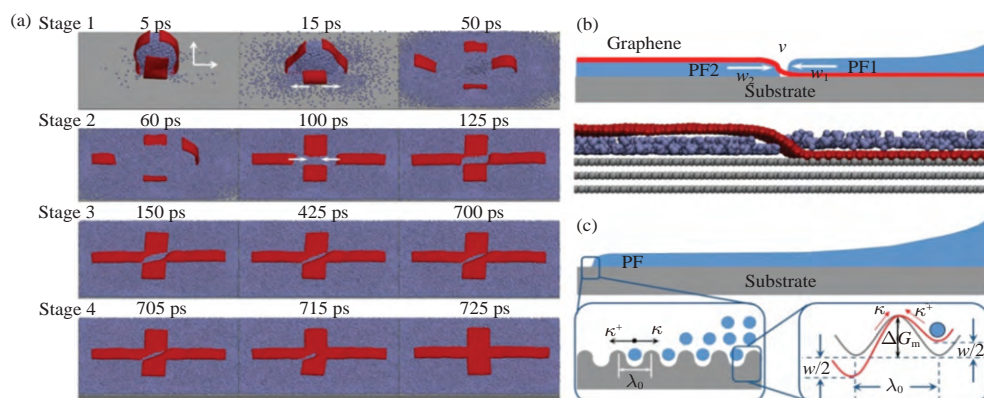

Fig. 9.   (a) Capillary wave propagation (borderline between red and ice blue) induced by the competition between PF1 and PF2 during which the graphene was delaminated from the substrate by PF2. (b) Competition between PF1 and PF2. (c) Schematic of the MKT. Silver, red, and ice blue atoms represent graphite, graphene, and water atoms, respectively.[46]

The properties of graphene–water interface under the electric field was further explored by Zhao's group with focus laid on the structure of the adsorbed water.[47] It was found that the adsorbed water on charged graphene experiences first-order ice-to-liquid (electromelting), and then liquid-to-ice (electrofreezing) phase transitions with the increase of the charge value (Fig. 10). The initial and final ice structures are incommensurate and commensurate with graphene, respectively. This novel phenomenon is attributed to the change of the water–water interactions from being attractive to repulsive at a critical charge value q_c. With the increase of the charge value, the strength of the attractive water–water interactions decreases below q_c, while the repulsive water–water interactions increases above q_c. These two inverse processes lead to electromelting and electrofreezing, respectively. To further investigate the dynamical properties of the adsorbed water, the transition state theory was extended by including both water–water interactions and water–graphene interactions in the Eyring equation. The theory and the simulations qualitatively agree well on the diffusion coefficient, the variation of which further confirms the ice–liquid–ice transition. This work not only expands our knowledge of graphene–water interface, but related analyses could also help recognize the controversial role of the surface charge or electric field in promoting phase transitions of water.

Although much progress has been made, there is still plenty of room for further investigation on the properties of graphene–water interfaces under electric field, e.g., other structures of the
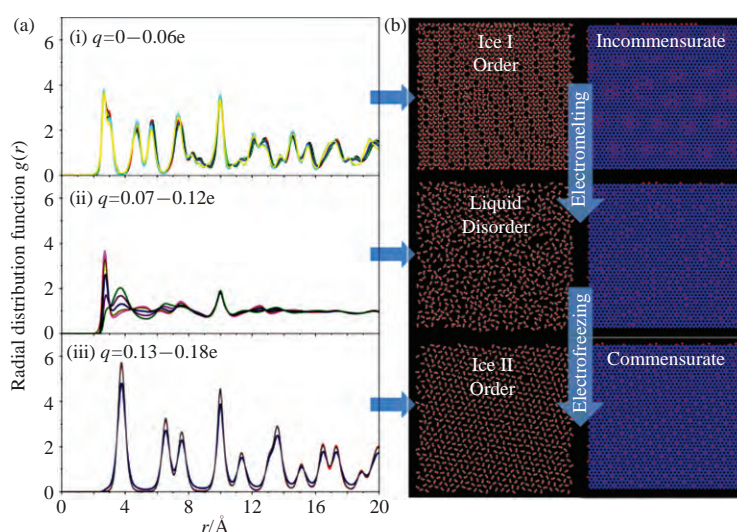
Fig. 10.   (a) Evolution of lateral oxygen-oxygen radial distribution function with respect to charge values q. (b) Structure of the adsorbed water on graphene. Red, white and blue atoms represent oxygen, hydrogen and carbon atoms, respectively. (i) $q = 0 - 0.06e$. Water molecules arrange in a hexagonal structure which is incommensurate with graphene. (ii) $q = 0.07 - 0.12e$. Water monolayer exhibits liquid state, the structure of which is disorder. (iii) $q = 0.13 - 0.18e$. Ice structure in this case is also hexagonal, but commensurate with graphene.

water overlayer on charged graphene would possibly reveal when the temperature is varied, and the influence of the phase transitions on the deformation of graphene would also be an interesting topic.

VI.   CELL SPREADING AS A MCL PROBLEM WITH EXTENDED MKT MODEL

Broadly speaking, cell spreading can be considered as a MCL problem. The complex biochemical reactions inside the cell are rate processes,[48] i.e., they are all related with time. As the traditional MKT was developed from absolute rate theory[18] and founded based on the same fact, rate process, it is reasonable to apply absolute rate theory to the field of biology, especially the cell–matrix biointerface. However, it is essential to note that molecule at the solid/liquid interface means molecule of liquid, while it represents molecule of protein at the cell–matrix biointerface, such as actin, integrin, cadherin, etc., as shown in Fig. 11. The molecule of liquid jumped between adjacent adsorption sites on the solid surface at the MCL corresponds to the reaction between receptor and ligand at the cell–matrix biointerface. Thus the application of absolute rate theory to cell adhesion, cell spreading and other cellular kinetics should be very careful, and relevant biological background is needed. Recently, Li et al.[49] have developed the absolute rate theory by taking into account the polymerization process of actin filament, established the dynamic equation of cell spreading, and extended the MKT to the field of cell–matrix biointerface. After reviewing the previous results of cellular kinetics, many theoretical models are found to be related with this extended molecular kinetic theory (eMKT).
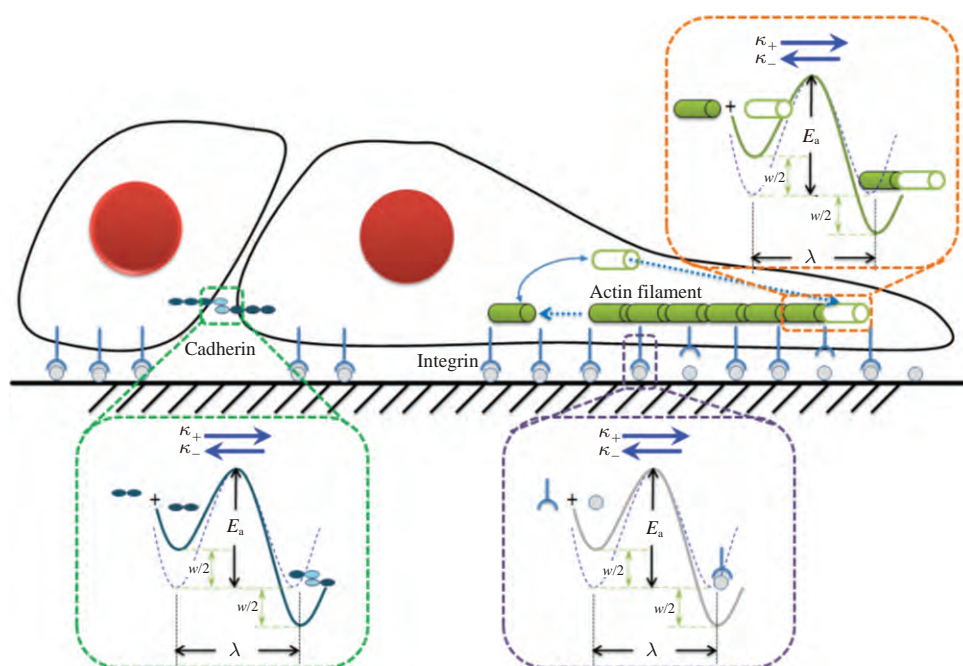
Fig. 11. The reaction process of actin, integrin, cadherin likely characterized by eMKT.

In the process of cell spreading, the change of cell morphology depends largely on the extension of pseodopods, and actin filament polymerization is the main cause of this extension. In Brownian ratchet model,[50] a polymerizing actin filament was modeled as a linear array of monomers; while, the ratchet mechanism is the intercalation of monomers between the barrier and the polymer tip. It is a confined diffusion problem, and the growth of filament relies on thermal fluctuation. While in the eMKT model of cell spreading established by Zhao's group,[49] this polymerization process was regarded as a chemical reaction of actin monomer adding onto the tip of filament, which is also affected by cell membrane and focal adhesion. It is not surprising that both models have the same form and Boltzmann factors, as long as we realize that actin polymerization is a Markov process. The addition of monomer onto the end of actin filament is an independent process, and has nothing to do with previous polymerization. The Brownian ratchet model was developed by considering the elastic deformation and the spatial distribution of actin filament,[51,52] and was applied to the research of cell spreading to obtain a scaling law between cell radius and time.[53] The adherens junction at the cell–cell interface was mediated by actin filament polymerization, and its kinetic process can also be characterized by this Brownian ratchet model.[54] Zhao's model[49] also predicted the scaling law in cell spreading, and further explained the different rigidity response of cell spreading on hydrogels and PDMS by introducing the influence of interfacial stiffness.

In the study of cell kinetics, the influence of substrate topography has not attracted much attention in theoretical modeling. This issue can be addressed by utilizing MKT, and will be the focus of theoretical analyses on cell–matrix biointerface.

VII. FUTURE DIRECTIONS

A water droplet with 2 mm in diameter contains approximately 1.4×10^{20} water molecules. A first-order emergent structure occurs as a result of shape interactions, e.g., hydrogen bonds in water molecules lead to surface tension of a droplet, as shown in Fig. 12. Therefore, wetting and dynamic wetting are emergent phenomena from bottom-up point of view. The MCL problem is still a wide-open field. The author would like to bring the following future directions of development to the readers.
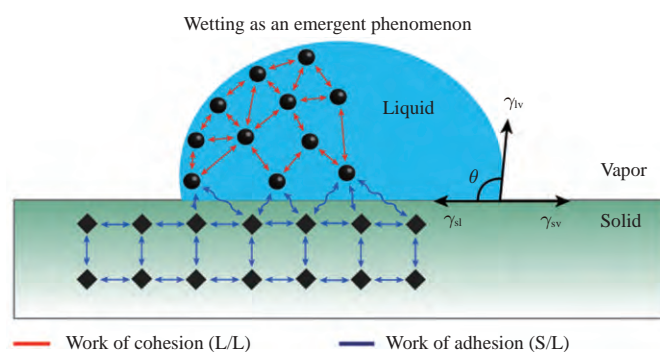

Fig. 12. Schematic of first-order emergent structure of wetting.

A. Stress singularity under multi-fields

Huh–Scriven paradox arises from 4 idealized assumptions: uncompressible Newtonian fluid, smooth solid surface, impenetrable solid–liquid interface, and nonslip boundary conditions, which all result in stress singularity at the MCL. When liquid spreading takes place under external fields, the situation is even worse. For example, driven by the Maxwell force caused by external electric field, the charges or dipoles in the liquid would concentrate at the MCL, which results in additional stress singularity at the MCL. We find out that PF is the first answer to the Huh–Scriven paradox in electrowetting. However, stress or energy dissipation singularity at the triple points under multi-fields is still a deep riddle in dynamic wetting.

B. Multiscale nature of dynamic wetting

The dynamic wetting process is essentially a multiscale problem. At microscopic level, PF, a thin molecular layer driven by the disjoining pressure, spreads ahead of the nominal MCL. We employ MKT to describe the dynamics of liquid. At macroscopic level, the liquid is driven by the hydrostatic pressure and does not spread until it reaches an equilibrium state described by Young's equation. We use hydrodynamics to describe the dynamic behaviors of liquid. At mesoscopic level, the liquid is governed by both the hydrostatic and the disjoining pressures. Microscopic motion described by MKT and macroscopic behavior described by hydrodynamics

should smoothly be connected at mesoscale.

Unraveling the atomic or molecular structure and the detailed interaction between the solid and liquid media at the solid–liquid interface is, therefore, one of the major challenges facing MCL problem today since it is only by understanding the physical and chemical processes involved in model systems that we can extrapolate to more complex environments.

C. Applications of EEC

The micro scale EEC devices can be fabricated by depositing metal (or other conductive material) electrodes upon soft cantilevers or membranes. By applying voltage to the electrodes, the deflection of the flexible devices, caused by droplet surface tension, can be controlled. EEC can be potentially used as a micro scale droplet encapsulation method or as an off-plane activation method for MEMS devices.

D. Cell spreading

In the theoretical models of cell kinetics, what we concerned most is to explain and predict cellular behaviors. Duo to the complexity of the experiments, the influence of substrate topography, the confined boundary condition, the dimensionality that cells feel and other factors should be considered in the further models. In addition, the kinetic behaviors of cell clusters which comprise cell–cell and cell–matrix interactions has not attracted much attention in theory, and could be a promising research direction.

E. Environmental and energy applications of the MCL problem

MCL has attracted considerable interest in the last several decades due to its inherently multiscale essence for us to thoroughly understand droplet dynamics, capillarity and wetting phenomena.[15,55–59] MCL has already been found in many environmental and energy applications, such as shale gas development,[60] energy harvest,[17] enhanced oil recovery (EOR),[61,62] and fuel cell fabrication.[63] Taking hydraulic fracture in shale as an example, the fracturing of rock by a pressurized liquid is also a solid–liquid–vapor MCL problem. In this sense, this review presents recent trends and future possibilities for MCL research and suggests which applications will see the most significant improvement.

1. Y. P. Zhao. Physical Mechanics of Surfaces and Interfaces. Science Press, Beijing (2012) (in Chinese).

2. T. Young. An essay on the cohesion of fluids. *Phil. Trans. Royal Soc. London* **95**, 65–87 (1805).

3. C. Huh, L. Scriven. Hydrodynamic model of steady movement of a solid/liquid/fluid contact line. *J. Colloid & Interface Sci.* **35**, 85–101 (1971).

4. P. G. de Gennes. Wetting: Statics and dynamics. *Rev. Mod. Phys.* **57**, 827–863 (1985).

5. P. G. de Gennes, F. Brochard-Wyart, D. Quéré. Capillarity and Wetting Phenomena: Drops, Bubbles, Pearls, Waves. Springer, New York (2004).

6. J. Berthier. Micro-Drops and Digital Microfluidics, 2nd edn. Elsevier, London (2013).

7. W. B. Hardy. The spreading of fluids on glass. *Phil. Mag.* **38**, 49–55 (1919).

8. W. Q. Ren, W. N. E. Boundary conditions for the moving contact line problem. *Phys. Fluids* **19**, 022101 (2007).

9. Q. Z. Yuan, Y. P. Zhao. Precursor film in dynamic wetting, electrowetting, and electro-elasto-capillarity. *Phys. Rev. Lett.* **104**, 246101 (2010).

10. H. Hervet, P. G. de Gennes. The dynamics of wetting: Precursor films in the wetting of "dry" solids. *C. R. Acad. Sci., Ser. II: Mec., Phys., Chim., Sci. Terre Univers* **299**, 499–503 (1984).

11. Q. Z. Yuan, Y. P. Zhao. Transport properties and induced voltage in the structure of water-filled single-walled boron-nitrogen nanotubes. *Biomicrofluidics* **3**, 022411 (2009).

12. C. Py, P. Reverdy, L. Doppler, et al. Capillary origami: spontaneous wrapping of a droplet with an elastic sheet. *Phys. Rev. Lett.* **98**, 156103 (2007).

13. P. Concus, R. Finn. On the behavior of a capillary surface in a wedge. *Proc. Natl. Acad. Sci. USA* **63**, 292–299 (1969).

14. C. X. Wang, S. H. Xu, Z. W. Sun, et al. A study of the influence of initial liquid volume on the capillary flow in an interior corner under microgravity. *Int. J. Heat Mass Tran* **53**, 1801–1807 (2010).

15. Q. Z. Yuan, Y. P. Zhao. Multiscale dynamic wetting of a droplet on a lyophilic pillar-arrayed surface. *J. Fluid Mech.* **716**, 171–188 (2013).

16. Q. Z. Yuan, Y. P. Zhao. Topology-dominated dynamic wetting of the precursor chain in a hydrophilic interior corner. *Proc. Royal Soc. A* **468**, 310–322 (2012).

17. Q. Z. Yuan, Y. P. Zhao. Hydroelectric voltage generation based on water-filled single-walled carbon nanotubes. *J. Am. Chem. Soc.* **131**, 6374–6376 (2009).

18. S. Glasstone, K. Laidler, H. Eyring. The Theory of Rate Processes. McGraw-Hill, New York (1941).

19. T. D. Blake, J. de Coninck. The influence of solid–liquid interactions on dynamic wetting. *Adv. Colloid Interface Sci.* **96**, 21–36 (2002).

20. H. Greenspan. On the motion of a small viscous droplet that wets a surface. *J. Fluid Mech.* **84**, 125–143 (1978).

21. C. D. Daub, D. Bratko, K. Leung, et al. Electrowetting at the nanoscale. *J. Phys. Chem. C* **111**, 505–509 (2007).

22. F. Mugele, J. Baret. Electrowetting: From basics to applications. *J. Phys.: Condens. Matter* **17**, R705 (2005).

23. J. Bico, B. Roman, L. Moulin, et al. Adhesion: Elastocapillary coalescence in wet hair. *Nature* **432**, 690 (2004).

24. X. Y. Guo, H. Li, B. Y. Ahn, et al. Two- and three-dimensional folding of thin film single-crystalline silicon for photovoltaic power applications. *Proc. Natl. Acad. Sci. USA* **106**, 20149–20154 (2009).

25. N. Patra, B. Y. Wang, P. Kral. Nanodroplet activated and guided folding of graphene nanostructures. *Nano Lett.* **9**, 3766–3771 (2007).

26. S. Jung, P. M. Reis, J. James, et al. Capillary origami in nature. *Phys. Fluids* **21**, 091110 (2009).

27. A. Antkowiak, B. Audoly, C. Josserand, et al. Instant fabrication and selection of folded structures using drop impact. *Proc. Natl. Acad. Sci. USA* **108**, 10400–10404 (2011).

28. M. Pineirua, J. Bico, B. Roman. Capillary origami controlled by an electric field. *Soft Matter* **6**, 4491–4496 (2010).

29. Z. Q. Wang, F. C. Wang, Y. P. Zhao. Tap dance of a water droplet. *Proc. Royal Soc. A* **468**, 2485–2495 (2012).

30. L. Bocquet, E. Charlaix. Nanofluidics, from bulk to interfaces. *Chem. Soc. Rev.* **39**, 1073–1095 (2010).

31. N. Tretyakov, M. Müllera. Correlation between surface topography and slippage: A molecular dynamics study. *Soft Matter* **9**, 3613–3623 (2013).

32. P. G. de Gennes. On fluid/wall slippage. *Langmuir* **18**, 3413–3414 (2002).

33. E. Lauga. Apparent slip due to the motion of suspended particles in flows of electrolyte solutions. *Langmuir* **20**, 8924–8930 (2004).

34. K. Falk, F. Sedlmerier, L. Joly, et al. Molecular origin of fast water transport in carbon nanotube membranes: superlubricity versus curvature dependent friction. *Nano Lett.* **10**, 4067–4073 (2010).

35. P. A. Thompson, S. M. Troian. A general boundary condition for liquid flow at solid surfaces. *Nature* **389**, 360–362 (1997).

36. F. C. Wang, Y. P. Zhao. Slip boundary conditions based on molecular kinetic theory: The critical shear stress and the energy dissipation at the liquid–solid interface. *Soft Matter* **7**, 8628–8634 (2011).

37. T. Schmatko, H. Hervet, L. Leger. Friction and slip at simple fluid–solid interfaces: The roles of the molecular shape and the solid–liquid interaction. *Phys. Rev. Lett.* **94**, 244501 (2005).

38. F. C. Wang, Y. P. Zhao. The unique properties of the solid-like confined liquid films: A large scale molecular dynamics simulation approach. *Acta Mech. Solida Sin*. **24**, 101–116 (2011).

39. D. M. Huang, C. Sendner, D. Horinek, et al. Water slippage versus contact angle: A quasiuniversal relationship. *Phys. Rev. Lett.* **101**, 226101 (2008).

40. O. I. Vinogradova. Slippage of water over hydrophobic surfaces. *Int. J. Miner. Process.* **56**, 31–60 (1999).

41. S. Lichter, A. Roxin, S. Mandre. Mechanisms for liquid slip at solid surfaces. *Phys. Rev. Lett.* **93**, 086001 (2004).

42. X. Yong, L. T. Zhang. Thermostats and thermostat strategies for molecular dynamics simulations of nanofluidics. *J. Chem. Phys.* **138**, 084503 (2013).

43. S. Ghosh, X. H. An, R. Shah, et al. Effect of 1-pyrene carboxylic-acid functionalization of graphene on its capacitive energy storage. *J. Phys. Chem. C* **116**, 20688–20693 (2012).

44. F. Yavari, C. Kritzinger, C. Gaire, et al. Tunable bandgap in graphene by the controlled adsorption of water molecules. *Small* **6**, 2535–2538 (2010).

45. Z. T. Li, Y. J. Wang, A. Kozbial, et al. Effect of airborne contaminants on the wettability of supported graphene and graphite. *Nature Mater*. **12**, 925–931 (2013).

46. X. Y. Zhu, Q. Z. Yuan, Y. P. Zhao. Capillary wave propagation during the delamination of graphene by the precursor films in electro-elasto-capillarity. *Sci. Rep.* **2**, 927 (2012).

47. X. Y. Zhu, Q. Z. Yuan, Y. P. Zhao, *Nanoscale* **6**, 5432–5437 (2014).

48. F. Chamaraux, S. Fache, F. Bruckert, et al. Kinetics of cell spreading. *Phys. Rev. Lett.* **94**, 158102 (2005).

49. J. Li, D. Han, Y. P. Zhao. Kinetic behaviour of the cells touching substrate: the interfacial stiffness guides cell spreading. *Sci. Rep*. **4**, 3910 (2014).

50. C. S. Peskin, G. M. Odell, G. F. Oster. Cellular motions and thermal fluctuations: the Brownian ratchet. *Biophys. J.* **65**, 316–324 (1993).

51. A. Mogilner, G. Oster. Cell motility driven by actin polymerization. *Biophys. J.* **71**, 3030–3045 (1996).

52. A. Mogilner, G. Oster. Force generation by actin polymerization II: The elastic ratchet and tethered filaments. *Biophys. J.* **84**, 1591–1605 (2003).

53. Y. Li, G. K. Xu, B. Li, et al. A molecular mechanisms-based biophysical model for two-phase cell spreading. *Appl. Phys. Lett.* **96**, 043703 (2010).

54. J. Brevier, M. Vallade, D. Riveline. Force-extension relationship of cell–cell contacts. *Phys. Rev. Lett.* **98**, 268101 (2007).

55. F. C. Wang, F. Q. Yang, Y. P. Zhao. Size effect on the coalescence-induced self-propelled droplet. *Appl. Phys. Lett.* **98**, 053112 (2011).

56. X. C. Qin, Q. Z. Yuan, Y. P. Zhao, et al. Measurement of the rate of water translocation through carbon nanotubes. *Nano Lett.* **11**, 2173–2177 (2011).

57. R. R. Nair, H. A. Wu, P. N. Jayaram, et al. Unimpeded permeation of water through helium-leak-tight graphene-based membranes. *Science* **335**, 442–444 (2012).

58. J. L. Liu, X. Q. Feng. On elastocapillarity: A review. *Acta Mech. Sin.* **28**, 928–940 (2012).

59. F. C. Wang, H. A. Wu. Pinning and depinning mechanism of the contact line during evaporation of nano-droplets sessile on textured surfaces. *Soft Matter* **9**, 5703–5709 (2013).

60. B. D. Lutz, A. N. Lewis, M. W. Doyle. Generation, transport, and disposal of wastewater associated with Marcellus Shale gas development. *Water Resour. Res.* **49**, 647–656 (2013).

61. F. C. Wang, H. A. Wu. Enhanced oil droplet detachment from solid surfaces in charged nanoparticle suspensions. *Soft Matter* **9**, 7974–7980 (2013).

62. F. C. Wang, H. A. Wu. Molecular dynamics studies on spreading of nanofluids promoted by nanoparticle adsorption on solid surface. *Theor. Appl. Mech. Lett.* **3**, 054006 (2013).

63. E. Gauthier, T. Hellstern, I. G. Kevrekidis, et al. Drop detachment and motion on fuel cell electrode materials. *ACS Appl. Mater. Interfaces* **4**, 761–771 (2012).

Zhao, Ya-Pu

Professor
State Key Laboratory of Nonlinear Mechanics (LNM)
Institute of Mechanics, Chinese Academy of Sciences
Beijing, China

Ya-Pu Zhao received his Ph.D. degree from Department of Mechanics, Peking University in 1994. He was promoted to full professor at the Institute of Mechanics, Chinese Academy of Sciences, in 1998. He obtained the "Distinguished Young Investigator Fund" from the National Natural Science Foundation in 2002. He served as the director of LNM during 2000−2005.

His main research interests include: Micro- and nano-mechanics, physical mechanics of surfaces and interfaces, mechanical problems in MEMS/NEMS, impact dynamics, etc. He is in the editorial board or advisory board of several international journals including Journal of Adhesion Science and Technology, Review of Adhesion and Adhesives, Friction, etc.

Selected Publications

- Y. P. Zhao. Nano and Mesoscopic Mechanics. Science Press, Beijing (2014) (in Chinese).

- Y. P. Zhao. Physical Mechanics of Surfaces and Interfaces. Science Press, Beijing (2012) (in Chinese).

- Q. Z. Yuan, Y. P. Zhao. Multiscale dynamic wetting of a droplet on a lyophilic pillar-arrayed surface. *Journal of Fluid Mechanics* **716**, 171−188 (2013).

- Z. Q. Wang, F. C. Wang, Y. P. Zhao. Tap dance of water droplet. *Proceedings of the Royal Society A* **468**, 2485−2495 (2012).

- F. C. Wang, F. Q. Yang, Y. P. Zhao. Size effect on the coalescence-induced self-propelled droplet. *Applied Physics Letters* **98**, 053112 (2011).

- Y. Zhang, Y. P. Zhao. Modeling nanowire indentation test with adhesion effect. *Journal of Applied Mechanics, Transactions of the ASME* **78**, 011007 (2011).

- Q. Z. Yuan, Y. P. Zhao. Precursor film in dynamic wetting, electrowetting and electro-elasto-capillarity. *Physical Review Letters* **104**, 246101 (2010). (cover image)

- Q. Z. Yuan, Y. P. Zhao. Hydroelectric voltage generation based on water-filled single-walled carbon nanotubes. *Journal of the American Chemical Society* **131**, 6374−6376 (2009).

- J. G. Guo, Y. P. Zhao. The size-dependent elastic properties of nanocrystals with surface effects. *Journal of Applied Physics* **98**, 074306 (2005).

- W. H. Lin, Y. P. Zhao. Nonlinear behavior for nanoscales electrostatic actuators with Casimir force. *Chaos, Solitons & Fractals* **23**, 1777−1785 (2005).

- Y. P. Zhao, L. Wang, T. Yu. Mechanics of adhesion in MEMS − a review. *Journal of Adhesion Science and Technology* **17**, 519−546 (2003).